Supplementary material for:

"Unraveling the pore-forming mechanism and thermokinetic behaviors of porous K-Ti co-doped Li_4SiO_4 pellets for efficient and stable CO_2 capture"

Yunlian Liu[1,2], Qian Jia[1,2], Mingkai Liu[1], Yuanhui Shen[1,2], Ruqi Zhang[1,2], Zihan Wan[1,2], Ying Pan[1*], Hongguang Jin[1]

[1] Institute of Engineering Thermophysics, Chinese Academy of Sciences, Beijing 100190, China

[2] University of Chinese Academy of Sciences, Beijing 100049, China

* To whom correspondence should be addressed.

E-mail address: panying@iet.cn

S1 Details of raw materials

Tabel S1. Source of precursor materials.

Reagents Name	Chemical formula	Quality index	Reagent purity	Supplier
Lithium carbonate	Li_2CO_3	Analytical pure	99.8%	Aladdin
Silicon dioxide	SiO_2	Analytical pure	99.5%	Aladdin
Potassium carbonate	K_2CO_3	Analytical pure	99.9%	Aladdin
Titanium dioxide	nano TiO_2	Analytical pure	rutile, 99.95%	Aladdin
α-cellulose fiber	$(C_6H_{10}O_5)_n$	Analytical pure	99.9%	Aladdin
Graphite powder	C	Analytical pure	99.9%	Aladdin
Polyvinyl alcohol	$(C_2H_4O)_n$	Analytical pure	99.9%	Aladdin
Polyethylene	$(C_2H_4)_n$	Analytical pure	99.9%	Best Chemical Technology Co., Ltd.
Deionized water	H_2O	Grade I	≥18MΩ·cm	-

S2 Thermal decomposition profiles of porogens

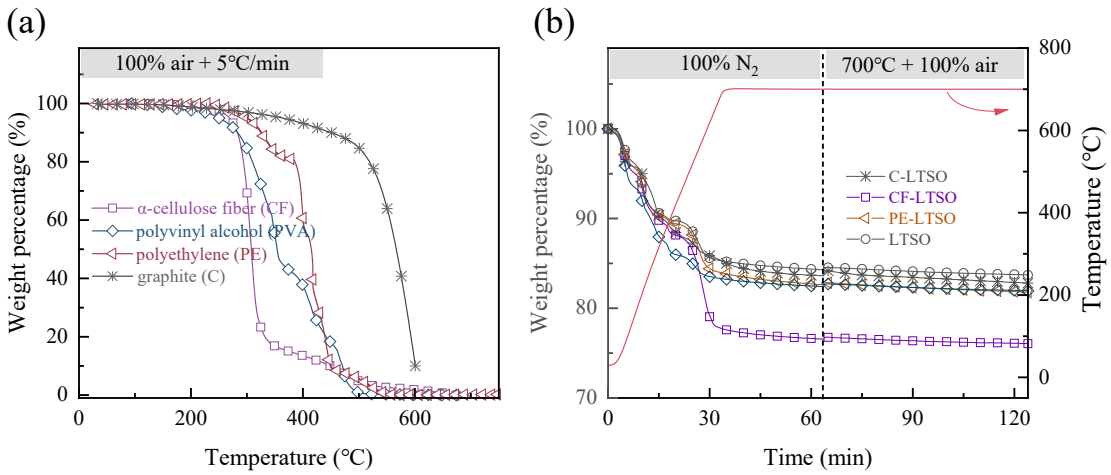

Fig. S1 (a) Thermogravimetric decomposition profiles of the pure porogens in an air atmosphere (5°C/min), (b) Dynamic weight loss curves of the calcined pellets containing different porogens during the calcination process (100% N_2 followed by 100% air).

S3 Setup for uniaxial compression testing

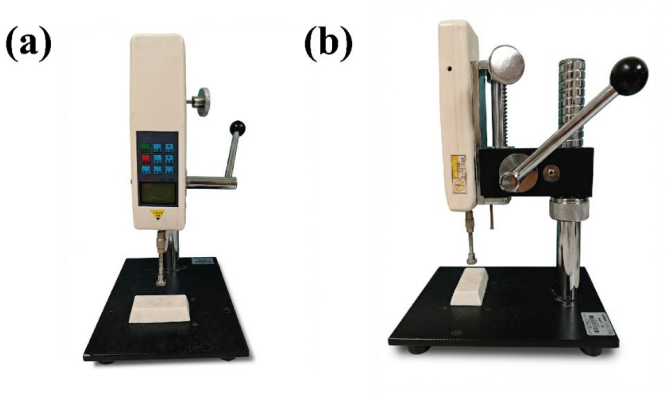

Fig. S2. Photographs of the experimental setup used for the uniaxial compression tests. Individual spherical pellets (1–1.5 mm in diameter, ~5 mg per pellet) were tested separately under stepwise uniaxial loading until fracture.

S4 Schematic of the custom-built attrition apparatus

The attrition resistance was evaluated using a custom-built cold-model attrition apparatus, schematically illustrated in Fig. S2. This apparatus was modified from a commercial Mini-S pelletizer (Xinyite, Shenzhen), where the original rotating plate was replaced with a smooth plate to primarily simulate surface abrasion.

The design, operating principles, and validation of this apparatus are identical to those reported in our previous work [1]. Consequently, the same testing protocol was adopted in this study, with adjustments only to the material loading amounts to suit the specific experimental requirements.

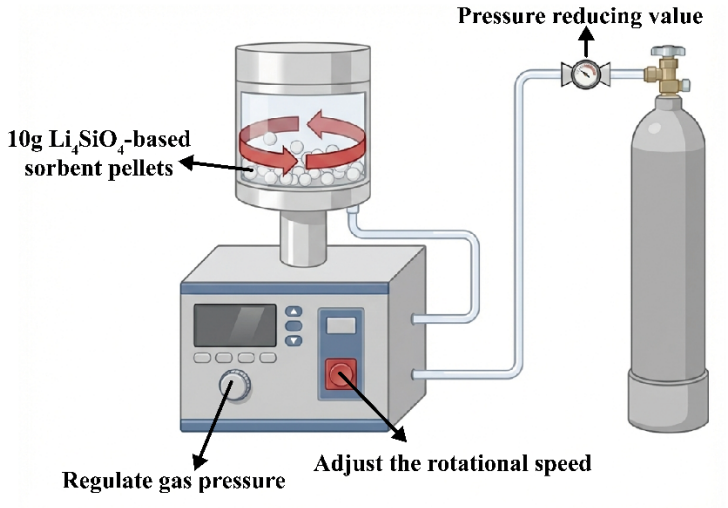

Fig. S3. Schematic illustration of the custom-built cold-state attrition test apparatus.

S5 Textural properties of fresh sorbents

Table S2 N_2 adsorption results of fresh Li_4SiO_4-based sorbent pellets with different porogens.

Label	BET surface area (m^2/g)	Pore volume (cm^3/g)	Average pore size (nm)	Crush load (N)
LTSO	0.3	0.6×10^{-2}	38.5	16.5
C-LTSO	1.9	2.0×10^{-2}	21.3	14.2
CF-LTSO	3.6	3.1×10^{-2}	22.1	15.9
PVA-LTSO	2.1	1.7×10^{-2}	20.5	22.1
PE-LTSO	4.4	3.3×10^{-2}	17.2	12.3

S6 Optimization of porogen loading amount

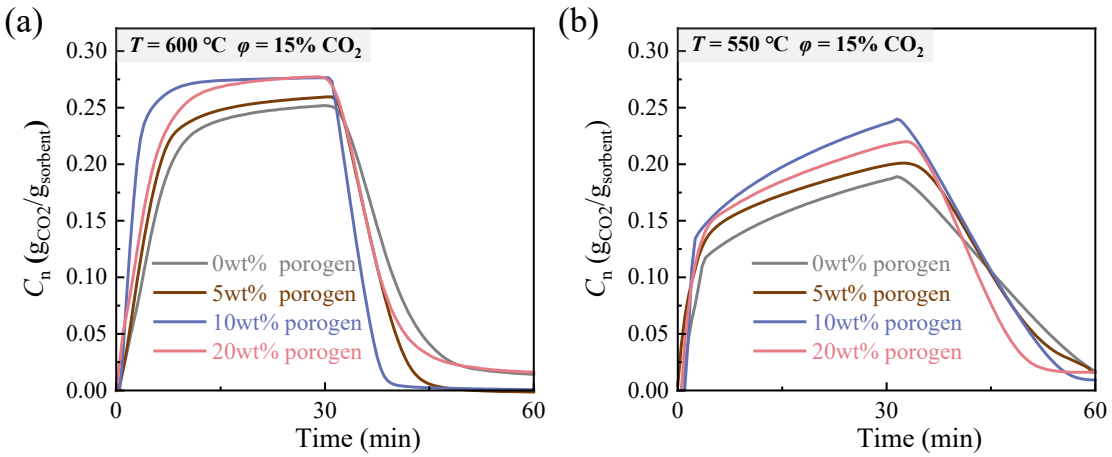

Fig. S4. Isothermal CO_2 uptake profiles of the CF-LTSO pellets synthesized with different porogen content.

Table S3 N_2 adsorption results of fresh CF-LTSO pellets with different porogen content.

Label	BET surface area (m^2/g)	Pore volume (cm^3/g)	Average pore size (nm)	Crush load (N)
0 wt%	0.3	0.6×10^{-2}	38.5	16.5
5 wt%	1.7	2.0×10^{-2}	20.3	16.1
10 wt%	3.6	3.1×10^{-2}	22.1	15.9
20 wt%	3.8	3.1×10^{-2}	16.4	13.3

S7 Kinetic parameters derived from double-exponential model

Table S4. Kinetic parameters calculated from sorbent isotherms at 600°C and different CO_2 partial pressures, fitted to a double-exponential model

Table	k_1	k_2	R^2
T = 500°C, φ = 15% CO_2			
CF-LTSO	3.7×10^{-1}	1.1×10^{-3}	0.99
C-LTSO	4.1×10^{-1}	8.0×10^{-4}	0.99
PVA-LTSO	3.5×10^{-1}	6.0×10^{-3}	0.99
PE-LTSO	3.5×10^{-1}	5.5×10^{-3}	0.99
LTSO	1.5×10^{-1}	3.0×10^{-4}	0.99
T = 550°C, φ = 15% CO_2			
CF-LTSO	6.3×10^{-1}	2.0×10^{-2}	0.98
C-LTSO	4.6×10^{-1}	1.3×10^{-2}	0.99
PVA-LTSO	6.3×10^{-1}	1.0×10^{-2}	0.98
PE-LTSO	6.5×10^{-1}	9.0×10^{-3}	0.98
LTSO	4.0×10^{-1}	7.9×10^{-3}	0.98
T = 600°C, φ = 15% CO_2			
CF-LTSO	1.0	2.5×10^{-2}	0.97
C-LTSO	5.3×10^{-1}	1.8×10^{-2}	0.96
PVA-LTSO	9.0×10^{-1}	1.8×10^{-2}	0.97
PE-LTSO	9.1×10^{-1}	1.6×10^{-2}	0.97
LTSO	4.5×10^{-1}	1.1×10^{-2}	0.98
T = 500°C, φ = 50% CO_2			
CF-LTSO	1.4×10^{-1}	1.5×10^{-3}	0.99
C-LTSO	2.5×10^{-1}	2.4×10^{-3}	0.99
PVA-LTSO	1.1×10^{-1}	2.2×10^{-3}	0.99
PE-LTSO	1.2×10^{-1}	2.0×10^{-3}	0.99
LTSO	9.0×10^{-2}	8.4×10^{-4}	0.98
T = 550°C, φ = 50% CO_2			
CF-LTSO	7.2×10^{-1}	8.6×10^{-2}	0.97
C-LTSO	6.2×10^{-1}	5.0×10^{-2}	0.96

PVA-LTSO	7.0×10^{-1}	8.3×10^{-2}	0.97
PE-LTSO	7.1×10^{-1}	8.3×10^{-2}	0.97
LTSO	4.5×10^{-1}	4.8×10^{-2}	0.98
T = 600°C, φ =50% CO_2			
CF-LTSO	1.1	1.9×10^{-1}	0.90
C-LTSO	1.2	3.3×10^{-1}	0.90
PVA-LTSO	8.8×10^{-1}	2.2×10^{-1}	0.94
PE-LTSO	9.3×10^{-1}	2.0×10^{-1}	0.94
LTSO	8.0×10^{-1}	1.6×10^{-1}	0.95

S8 Thermodynamic equilibrium calculations (HSC Chemistry)

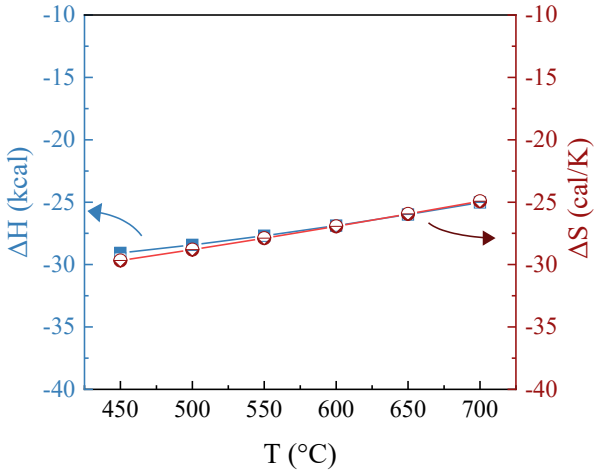

Fig.S5 Theoretical variations of reaction enthalpy (Δ*H*) and entropy (Δ*S*) for the carbonation of as a function of temperature, calculated using HSC Chemistry 9.0.

S9 Phase evolution analysis (XRD) of cycled sorbents

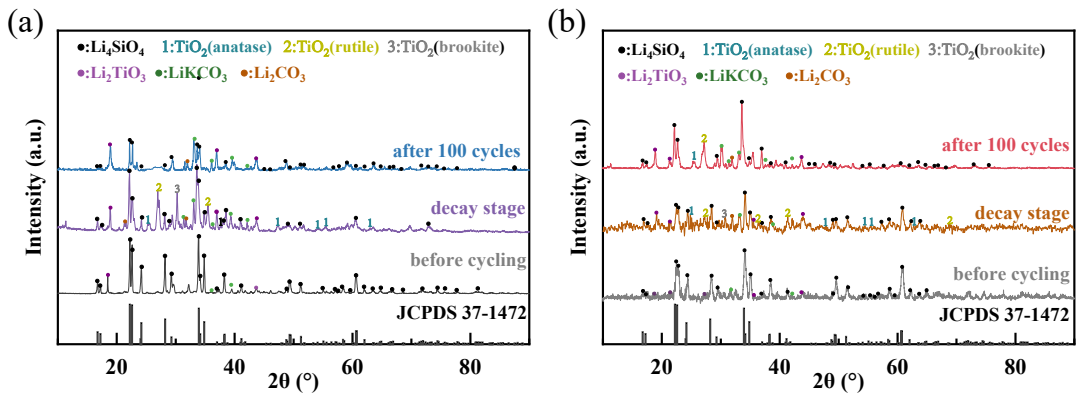

Fig. S6. XRD pattern of (a)PVA-LTSO and (b)LTSO sorbent particle at different stages.

S10 Mechanical strength evolution during cycling

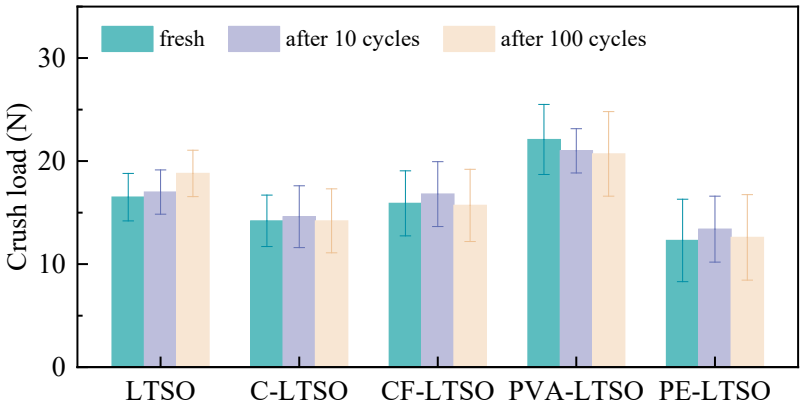

Fig. S7. Crushing strength of the different sorbent pellets.

Reference

[1] M. Liu, Z. Wan, Y. Liu, Q. Jia, R. Zhang, Y. Li, Y. Pan, H. Jin, Fe-Ni oxygen carrier particles for mid-temperature natural gas chemical looping reforming: Mechanism and large-scale performance, Chem. Eng. J. 527 (2026) 171721. https://doi.org/10.1016/j.cej.2025.171721.